

A comparison of magnetohydrodynamic instabilities at the Martian ionopause

T. Penz ^{a,b,*}, I.L. Arshukova ^c, N. Terada ^d, H. Shinagawa ^d, N.V. Erkaev ^c,
H.K. Biernat ^{a,b,e}, H. Lammer ^a

^a Space Research Institute, Austrian Academy of Sciences, Schmiedlstr. 6, A-8042 Graz, Austria

^b Institute of Physics, Division for Theoretical Physics, University of Graz, Universitätsplatz 5, A-8010 Graz, Austria

^c Institute for Computational Modelling, Russian Academy of Sciences, 660036 Krasnoyarsk-36, Russia

^d Solar–Terrestrial Environment Laboratory, Nagoya University, Japan

^e Institute for Geophysics, Astrophysics, and Meteorology, University of Graz, Universitätsplatz 5, A-8010 Graz, Austria

Received 23 September 2004; received in revised form 4 November 2004; accepted 4 November 2004

Abstract

It is known from Pioneer Venus measurements that at the Venusian ionopause wave-like structures develop, which can detach in the form of ionospheric plasma clouds. This phenomenon is assumed to occur due to the Kelvin–Helmholtz instability, which can appear in large regions of the Venusian ionopause. Recent studies of Mars Global Surveyor measurements indicate that wave-like structures and plasma clouds also detach from the Martian ionopause. Therefore, these features seem to be common for the solar wind interaction of non-magnetized planets. We study the conditions at the Martian ionopause with respect to the occurrence of several MHD instabilities. The conditions in the magnetosheath are modeled by a semi-analytical MHD simulation that includes mass loading. The ionospheric parameter needed for the model calculations are taken from a global hybrid model. The stability of the Martian ionopause against the Kelvin–Helmholtz, the Rayleigh–Taylor, and the interchange instability is analyzed. Further, we suggest that including the Hall term in the description of the Kelvin–Helmholtz instability gives a current in the planetary boundary layer resulting in a shear flow compared with the ionospheric plasma, which can lead to an unstable boundary layer near the subsolar point. Since the interchange instability depends on the curvature of the magnetic field lines, we additionally study the influence of the strong curvature of the Martian ionopause due to the localized, remnant, crustal magnetism appearing mainly in the southern hemisphere of Mars.

© 2004 COSPAR. Published by Elsevier Ltd. All rights reserved.

Keywords: Instabilities; Mars; Atmospheric loss; Magnetohydrodynamics

1. Introduction

Measurements of the Pioneer Venus Orbiter (PVO) spacecraft revealed a number of characteristic ionospheric structures that may be signatures of solar wind–ionosphere interaction processes (e.g., [Brace et al.](#)

[al., 1982](#); [Russell et al., 1982](#)). Among them are wavelike plasma irregularities, found at the top of the dayside ionosphere and plasma clouds observed above the ionopause, primarily near the terminator and further downstream. The detailed analysis of several plasma clouds has shown that the plasma within the clouds themselves is ionosphere-like in electron temperature and density ([Brace et al., 1982](#)). When such plasma clouds were seen far above the ionosphere, they were clearly separated by an intervening region of magnetosheath plasma. This

* Corresponding author. Tel.: +43 316 4120 635; fax: +43 316 4120 690.

E-mail address: thomas.penz@oeaw.ac.at (T. Penz).

large separation in a direction perpendicular to the magnetosheath flow suggests that the ionospheric plasma in the clouds must have originated in the ionosphere upstream on the dayside, indicating that magnetohydrodynamic (MHD) instabilities may occur at the Venusian ionopause, which was first suggested by Wolff et al. (1980). Elphic and Ershkovich (1984) analyzed the stability of the Venusian ionopause by using one-fluid MHD equations for a perfectly conducting, incompressible, inviscid fluid, and concluded that the Kelvin–Helmholtz instability is the dominant instability over most of the dayside ionopause. After that, the Venusian solar wind–ionosphere interaction was analyzed using analytical (e.g., Cloutier et al., 1983; Elphic and Ershkovich, 1984) and numerical models (e.g., Thomas and Winske, 1991). Recently, Terada et al. (2002) used a global hybrid simulation to describe the Kelvin–Helmholtz instability at Venus.

Elphic and Ershkovich (1984) mentioned that under certain circumstances, the interchange instability can also develop at the Venusian ionopause. The interchange instability is similar in nature to the Rayleigh–Taylor instability in classic hydrodynamic, where the magnetic tension plays the role of an effective gravitational force (Chandrasekhar, 1961). In space plasma, there exist structures which have thin, curved boundary layers separating magnetic fields and plasmas of different origin. Magnetospheres of planets and magnetic clouds are typical examples of such structures. The interchange instability was proposed as an important process occurring at the Earth's magnetopause (Rezhnev and Maltsev, 1994). Recently, Arshukova et al. (2004) showed that the Venusian ionopause can also be subject to the interchange instability.

The global scale Martian solar wind interaction operates similar to that at the ionosphere/atmosphere of Venus (e.g., Ma et al., 2002). Acuña et al. (1998) reported the detection of cold electrons above the Martian ionopause, indicating the presence of detached plasma clouds in the magnetosheath of Mars. Penz et al. (2004) investigated the Kelvin–Helmholtz instability at the Martian ionopause and discussed the influence on ion loss from Mars.

In the present study, we use the global hybrid model from Terada et al. (2004) to derive the ionosphere composition at Mars. This minimizes uncertainties regarding the ionopause altitude and the particle density, which were discussed in Penz et al. (2004). The magnetosheath conditions are modeled by an MHD approximation which we have applied successfully to the case of the solar wind flow around Venus (Biernat et al., 2001). This approach is partly analytical and partly numerical. We use this combined approach because the hybrid model provides the ionospheric composition better than previous estima-

tions used in Penz et al. (2004), but the MHD approach gives the magnetosheath parameters in an analytical representation which is needed as an input parameter for the analysis of the Kelvin–Helmholtz instability in Hall–MHD. The instability growth rates are calculated by using one-fluid MHD equations for a perfectly conducting, incompressible, inviscid fluid (Elphic and Ershkovich, 1984). Additionally, the Kelvin–Helmholtz instability is analyzed in the frame of Hall–MHD at Mars for the first time. Also the influence of a strong local curvature of the Martian ionopause due to crustal magnetism (Ma et al., 2002) is discussed.

2. Modeling the Martian ionosphere composition

The 2-D global hybrid model that self-consistently includes a planetary ionosphere developed for the Venus–solar wind interaction studied by Terada et al. (2002) is applied to the Martian solar wind interaction. The hybrid model treats electrons as a massless fluid, while solving motions of ions. O^+ , O_2^+ , CO_2^+ , and H^+ ion species, and related chemical reactions and collisions between ion–ion, ion–neutral, ion–electron, electron–ion, and electron–neutral are considered in the model. Chemical reactions and collisions of particle ions are implemented by a Monte–Carlo method. Altitude profiles of the atmospheric models used as input are taken from the atmospheric models used in Shinagawa and Cravens (1989) for Viking conditions. Ionization rates are calculated for each neutral for each period. These production rates are assumed to be proportional to the cosine of the solar zenith angle on the dayside. The exospheric neutrals are subject to photoionization, electron impact ionization, and charge exchange reactions. These reaction rates as well as the collision frequencies and chemical reaction rates for ions used are the same as those listed in Terada et al. (2002). From this model it is possible to find the ionospheric densities in the region near the ionopause (we assume that the ionopause corresponds to an electron density of 100 cm^{-3}). For $SZA = 0^\circ$, the ionopause height is about 370 km, and the main ion is O^+ with a density of about 100 cm^{-3} , while the second important ion is H^+ with a density 5 times less than for O^+ (Fig. 1, left panel). For $SZA = 90^\circ$, the ionopause height is found to be about 250 km. At this height, three ions, namely O_2^+ , O^+ , and H^+ , have nearly the same particle density of about 30 cm^{-3} (Fig. 1, right panel). The magnetic field strength near the ionopause is calculated self-consistently from the model and is found to be about 30 nT (Terada et al., 2004). We should keep in mind that the values mentioned above can vary depending on solar wind parameters, but the uncertainties regarding the location of the ionopause in the terminator region discussed in Penz et al. (2004) can be minimized by using the model results.

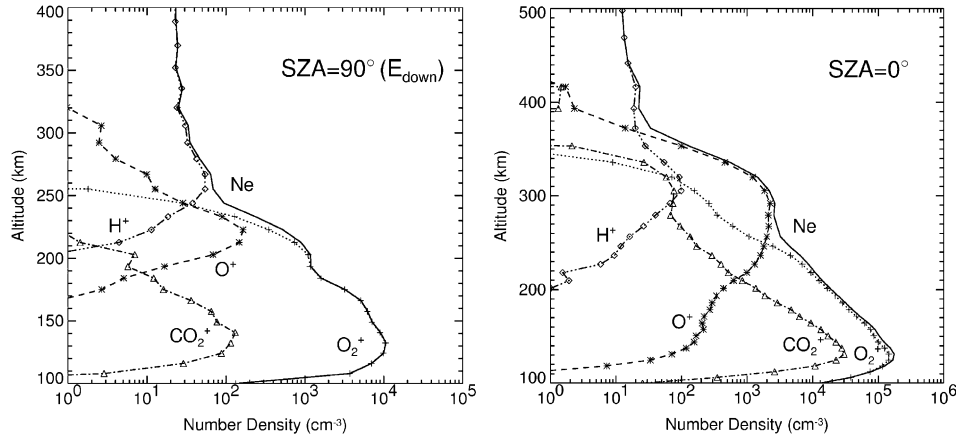


Fig. 1. Particle densities in the Martian ionosphere for SZA = 0° (right panel) and SZA = 90° (left panel).

3. The magnetosheath model

Considering a steady-state situation, we model the plasma in a planetary magnetosheath as a non-dissipative fluid which obeys the standard ideal MHD equations extended for mass loading processes (Biernat et al., 2001). There are corresponding boundary conditions at the ionopause. We model this boundary as a tangential discontinuity satisfying the condition that there exist no normal components of the velocity and the magnetic field across the boundary. Additionally, we introduce quantities normalized to the solar wind parameter (Biernat et al., 2001). For this case, the MHD equations can be written in the following form (Penz et al., 2004):

$$\rho(\mathbf{U} \cdot \nabla)\mathbf{U} + \nabla\Pi = \varepsilon(\mathbf{B} \cdot \nabla)\mathbf{B} - q(\mathbf{R})\mathbf{U},$$

$$\nabla \cdot (\rho\mathbf{U}) = q(\mathbf{R}),$$

$$\nabla \cdot \mathbf{B} = 0, \quad \nabla \times (\mathbf{U} \times \mathbf{B}) = 0,$$

$$\nabla \cdot \left\{ \left[\frac{1}{2}\rho U^2 + \frac{\kappa}{\kappa-1}P \right] \mathbf{U} + \varepsilon\mathbf{B} \times (\mathbf{U} \times \mathbf{B}) \right\} = 0 \quad (1)$$

with

$$\Pi = P + \varepsilon B^2/2.$$

Here, \mathbf{U} is the bulk velocity, P is the plasma pressure, and \mathbf{E} and \mathbf{B} are the electric and magnetic field, respectively, and $\varepsilon = B_{\text{sw}}^2/(4\pi\rho_{\text{sw}}U_{\text{sw}}^2)$. We introduced a normalized ion source function

$$q(\mathbf{R}) = q_0 \exp\left(\frac{R_0 - R}{H_0}\right), \quad (2)$$

where H_0 is the scale height of oxygen. The mass loss parameter q_0 is given as

$$q_0 = \frac{Sm_0R_0}{\rho_{\text{sw}}U_{\text{sw}}}, \quad (3)$$

where the ion production term is $S = N_0s = 5.85 \times 10^{-3} \text{ cm}^{-3} \text{ s}^{-1}$ (Lichtenegger et al., 2002), m_0 is the mass of the neutral particles, and ρ_{sw} and U_{sw} denote the solar wind density and velocity, respectively. By using $R_0 = 3693 \text{ km}$ we achieve a typical value for the mass loading parameter of $q_0 \sim 0.5$ (Penz et al., 2004).

We integrate the MHD equations after bringing them to a special form, called string equations. The numerical scheme is based on the Lax–Wendroff method. We use a simplifying assumption concerning the behavior of the total pressure. In our method, its variation along the ionopause surface obeys the well-known Newtonian formula. Using this method it is possible to find the density and velocity along stream lines in the magnetosheath over the Martian ionopause. In Fig. 2 results of the model calculations are shown. From top to bottom, the first two panels show variations of the mass density and the total velocity along different stream lines (1–9) at the ionospheric boundary. The corresponding stream lines are shown at the bottom panel. Each stream line starts from the stagnation line and goes along the ionopause. The stream line number 9 corresponds to the ionopause in the XY -plane for $Z = 0$, while stream line number 1 corresponds to a flow nearly directed to the polar terminator. Near the subsolar point we find that the magnetosheath velocity tends to zero, while the mass density increases to about 2.5 times the solar wind mass density. Near the terminator, the flow velocity is found to be about 0.3 times the solar wind velocity, while the mass density is the same as in the solar wind. For a nominal solar wind velocity of 400 km/s, the magnetosheath velocity is about 120 km/s. This result is in good agreement with the global hybrid model which leads to velocities in the order of 100 km/s in the vicinity of the polar terminator. The largest flow velocities are found at the equatorial flanks, where they are in the range of the solar

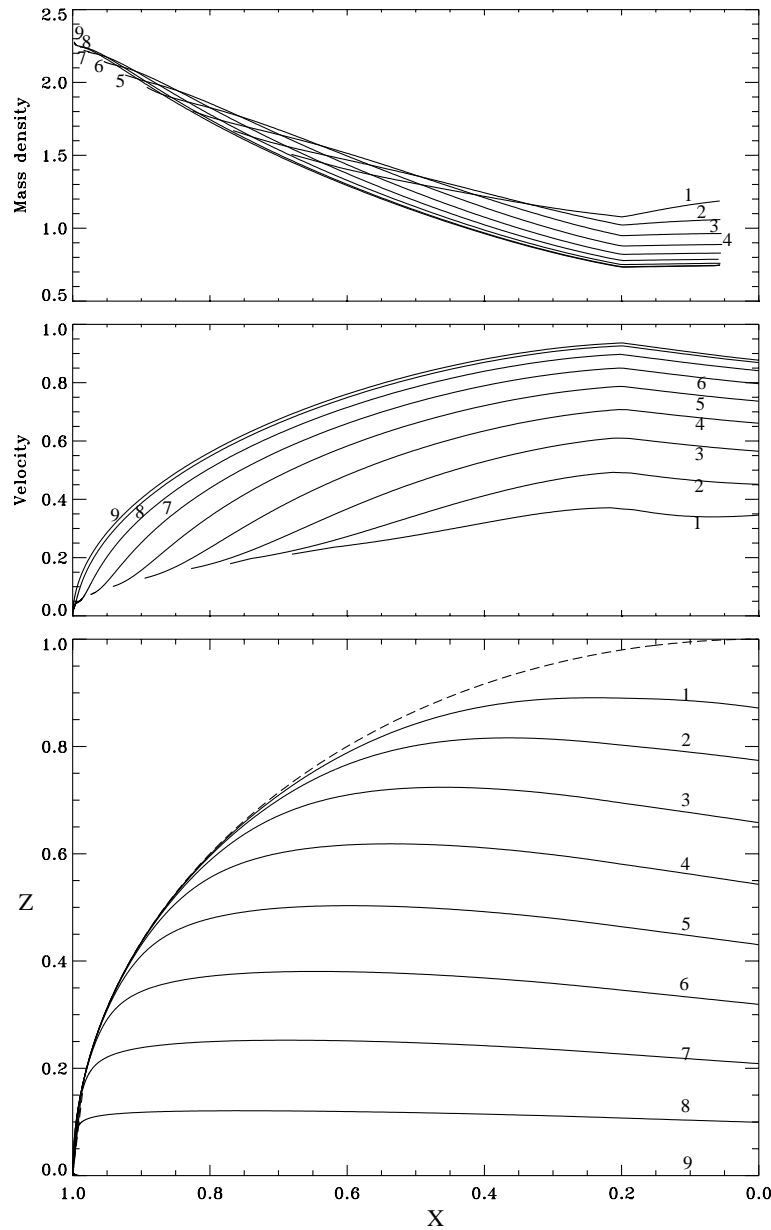


Fig. 2. From top to bottom: the first panel shows the mass density variations along different stream lines near the ionopause; the second panel gives the total velocity variation along different stream lines; the last panel shows the stream lines along the ionopause, where the dashed line indicates the shape of the obstacle in the XZ -plane. The X -direction points from Mars to the Sun, while Z is directed parallel to the IMF direction. $X = 0$ is the center of the planet, while $X = 1$ corresponds to the subsolar point of the ionopause. The velocity and the mass density are normalized with respect to solar wind quantities.

wind velocity. Also the mass density is in the range of the solar wind density in this region.

4. Analysis of the Kelvin–Helmholtz instability

Penz et al. (2004) investigated the occurrence of the K–H instability at the Martian ionopause using the ideal MHD approach developed by Wolff et al. (1980), but

pointed out that there are many uncertainties regarding the ionospheric parameters used in the model. The instability growth rate is found as

$$\gamma = \left(k^2 \frac{\rho_1 \rho_2 (U_2 - U_1)^2}{(\rho_1 + \rho_2)^2} + 2|k^3| \frac{(v_1 + v_2) \rho_1 \rho_2 (U_2 - U_1)}{(\rho_1 + \rho_2)^2} - k^4 \left(\frac{v_2 \rho_2 - v_1 \rho_1}{\rho_1 + \rho_2} \right)^2 - |k| \frac{g(\rho_2 - \rho_1)}{\rho_1 + \rho_2} \right)^{1/2}, \quad (4)$$

where U and ρ denote the plasma velocity and the plasma density, subscripts 1 and 2 denote magnetosheath and ionospheric conditions, respectively, g is the gravitational acceleration at the ionopause, and ν is the viscous coefficient. In this work we use ionospheric densities as shown in Fig. 1, while the magnetosheath conditions are found from Fig. 2. From the global hybrid model, the flow velocity in the ionosphere is found to be less than several km/s, therefore U_2 can be safely neglected in Eq. (4).

For the region near the subsolar point the flow velocity in the magnetosheath is very small, leading to an instability growth rate which is much smaller than the characteristic time scale in the system, therefore this region is stable with respect to the K–H instability in ideal MHD. As the characteristic time scale, we use the magnetic barrier formation time

$$T_m = \frac{\Delta_s}{U_s} \ln \frac{\Delta_s}{\delta_p}, \quad (5)$$

where Δ_s is the magnetosheath thickness, U_s is the solar wind velocity downstream of the bow shock, and δ_p is a distance comparable with the proton plasma scale (Arshukova et al., 2004). For a solar wind velocity of 400 km/s, the magnetic barrier formation time is 40 s, and for a solar wind velocity of 250 km/s, it is 63 s. If the instability growth time is smaller than this characteristic timescale, the instability will evolve into a non-linear stage, allowing the detachment of plasma clouds.

If we consider the terminator region for $\text{SZA} = 90^\circ$, the ionospheric mass density is about 1500 cm^{-3} . For nominal solar wind velocities of about 400 km/s, the maximum instability growth rate is 0.1 s^{-1} for wavelength of 50 km. But also for a larger wavelength of 100 km the growth rates are $6 \times 10^{-2} \text{ s}^{-1}$, giving an instability growth time of 16 s, which is well below the characteristic timescales. For a low solar wind velocity of 250 km/s, the maximum growth rate appears for the same wavelength than for nominal solar wind velocities, but the growth rates are about half the values for nominal solar wind velocity. Therefore, it is more likely that the K–H instability appears for nominal solar wind conditions. Near the equatorial flanks, we assume that the ionosphere composition is the same than near the terminator, but the magnetosheath conditions differ significantly from the values at the terminator (Penz et al., 2004). For a nominal solar wind velocity of 400 km/s, the flow velocity in the magnetosheath is 360 km/s, giving a maximum growth rate of 0.15 s^{-1} at wavelength slightly more than 100 km, which corresponds to a growth time of 7 s. For a low solar wind velocity, the maximum growth rate of 0.35 s^{-1} occurs for wavelength of about 40 km, which is not in agreement with the finite boundary condition by Ong and Roderick (1972), that the wave number k for the maximum instability growth

rate must satisfy the condition $ka/2 \approx 0.5$, where a is the thickness of the boundary layer. For wavelength of 100 km, the growth rate is 0.2 s^{-1} and the growth time is 5 s.

Radio occultation measurements of the ionopause altitude by Kliore (1992) showed that the ionopause altitude tends to decrease with increasing SZA. Also the global hybrid model used in this work shows that the ionopause altitude for high SZA is located in a region where collisions become important during low solar wind velocity conditions. In this case, two difficulties arise. Firstly, the shape of the ionopause is assumed to slightly increase in the MHD model, while observations (Kliore, 1992) and the hybrid model indicate that it is slightly decreasing. However, this difference becomes significant for large SZA ($\text{SZA} > 90^\circ$), which are not considered in this paper. For smaller SZA, the difference between the ionopause shapes in the models is less significant and therefore can be neglected in our rough estimation. The second implication is that the hybrid model shows that the decrease of the ionopause for large SZA leads to a dissipation of the Kelvin–Helmholtz instability for $\text{SZA} > 100^\circ$. Therefore, the evolution of the Kelvin–Helmholtz instability for large SZA should be studied in more detail in future. Additionally, it should be mentioned that the Kelvin–Helmholtz instability occurs also in the global hybrid simulation applied to Mars, but as already discussed in Terada et al. (2002) for Venus, the resolution of the hybrid model does not allow us to determine the wavelength exactly, therefore the analytical approach is used in this work.

5. The Kelvin–Helmholtz instability in Hall-MHD

In this section, we analyze the Kelvin–Helmholtz instability using the Hall-MHD equations

$$\frac{\partial \mathbf{U}}{\partial t} + (\mathbf{U} \cdot \nabla) \mathbf{U} + \frac{1}{\rho} \nabla P = -\frac{1}{c\rho} (\mathbf{J} \times \mathbf{B}),$$

$$\mathbf{E} + \frac{1}{c} (\mathbf{U} \times \mathbf{B}) = \frac{1}{nec} (\mathbf{J} \times \mathbf{B}),$$

$$\nabla \times \mathbf{E} = -\frac{1}{c} \frac{\partial \mathbf{B}}{\partial t}, \quad \nabla \times \mathbf{B} = \frac{4\pi}{c} \mathbf{J},$$

$$\nabla \cdot \mathbf{U} = 0, \quad \nabla \cdot \mathbf{B} = 0. \quad (6)$$

In Hall-magnetohydrodynamics, the Kelvin–Helmholtz instability can occur in a current region when the current is related to the sheared cross field ion flow given as $\mathbf{J} = ne\mathbf{U}$. We consider the subsolar Martian ionopause where the background plasma velocity is practically equal to zero. In order to obtain an analytical solution, we use a simplified model with piece-wise constant parameters as a first approach for the estimation of the instability growth rate. A similar approach was used

by Arshukova et al. (2004) to calculate the growth rate of the interchange instability at the subsolar ionopause of Venus. As it was shown there, a piece-wise constant approximation gives slightly overestimated result for the growth rate. We consider three regions: the ionosphere (region 0), the current layer (region 1) and the transition layer (region 2), which can be seen in Fig. 3. Since the plasma density inside the subsolar Martian ionosphere is about 1600 cm^{-3} , it is much larger than the plasma density of the solar wind. Therefore, we suppose in our consideration that the ratio between the ionosphere density and the solar wind density goes to infinity. As a result we obtain a dispersion equation with solutions given as

$$\omega_{1,2} = Uk \frac{\rho_1(e^{2ka} + 1)}{\rho_1(e^{2ka} + 1) + \rho_2(e^{2ka+1})} \pm iUk \times \frac{\sqrt{\rho_1\rho_2(e^{4ka} - 1)}}{\rho_1(e^{2ka} + 1) + \rho_2(e^{2ka} - 1)}. \quad (7)$$

In Fig. 4, the dependency of the frequency and the growth rate of the instability on the thickness of the current layer is shown. One can see from this figure that an increase of the growth rate occurs for a decreasing thickness of the current layer. The current is becoming stronger and the instability is more pronounced. Fig. 5 shows

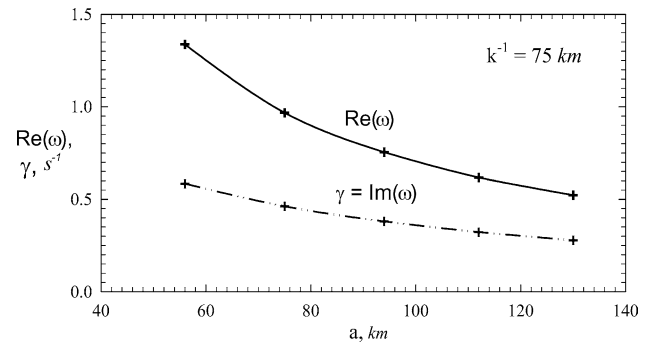


Fig. 4. The frequency and the growth rate of the instability as a function of the current sheath thickness.

the instability growth rate as a function of the parameter ka for different thicknesses of the layer. It is shown that for a thin current layer, the growth rate is higher compared with a thicker current sheet. For the conditions at the subsolar point, the ionopause thickness is about $a = 100 \text{ km}$, the curvature radius is $R = 3750 \text{ km}$, the plasma densities are $\rho_1 = 50 \text{ cm}^{-3}$ and $\rho_2 = 15 \text{ cm}^{-3}$, and $k^{-1} = 75 \text{ km}$, the growth rate of the instability is about 0.38 s^{-1} . This corresponds to an instability growth time of about 3 s, which is much less than the

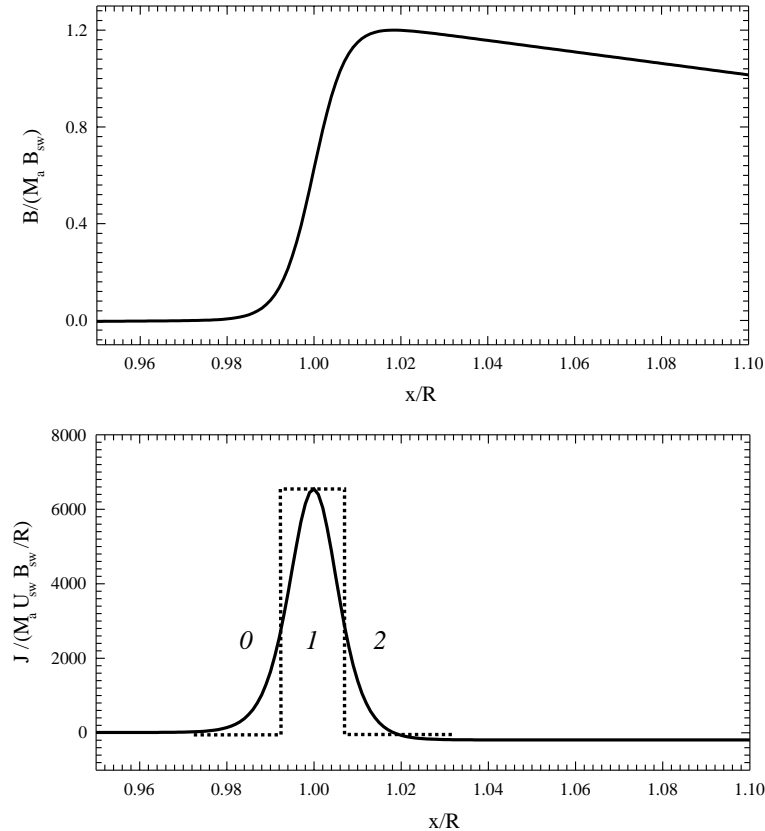


Fig. 3. Approximation for the magnetic field (upper panel) and the electric current (lower panel) in normalized quantities. The numbers refer to the different regions described in the text.

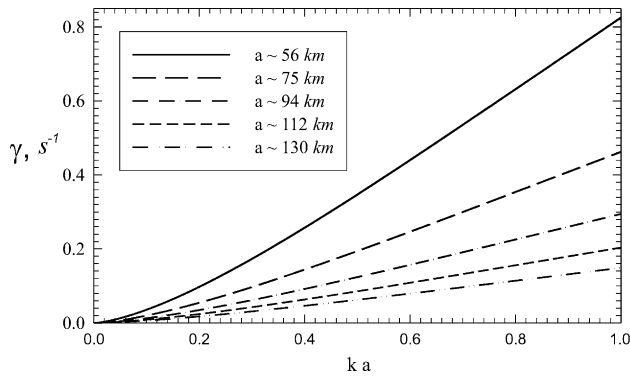


Fig. 5. The instability growth rate for different current sheet thicknesses. The smaller the current layer, the higher the growth rate.

time scale of the magnetic barrier formation. Therefore, the Martian ionopause may be unstable against the Kelvin–Helmholtz instability also at the subsolar point if we apply Hall-MHD. Nevertheless, the influence of gravity should be considered in further work on this topic.

6. The interchange instability and the influence of crustal magnetism

In the investigation of different instabilities occurring at Venusian ionopause Elphic and Ershkovich (1984) also considered the interchange instability in the frame of an ideal MHD treatment. Recently, Arshukova et al. (2004) discussed this instability at the Venusian ionopause including finite boundary effects and found that it is likely that the interchange instability appears. In this work we will use the analytical formula derived by Elphic and Ershkovich (1984), where the classical Rayleigh–Taylor instability as well as the interchange instability due to centrifugal forces and the magnetic curvature effects are included

$$\gamma^2 = k \frac{g(\rho_2 - \rho_1)}{\rho_1 + \rho_2} + k \frac{\rho_1 U_1^2 - \rho_2 U_2^2}{(\rho_1 + \rho_2) R_c} - k \times \frac{B_2^2 - B_1^2}{4\pi(\rho_1 + \rho_2) R_m}, \quad (8)$$

where subscripts 1 and 2 denote magnetosheath and ionosphere parameters, respectively. R_m denotes the magnetic curvature radius, while R_c describes the curvature for the centrifugal force. At the subsolar point, the flow velocity in the magnetosheath is very small, therefore we neglect the influence of the centrifugal term in the equation above. Using a magnetic field strength of $B_1 = B_2 = 30$ nT and $R_c = R_m = 3750$ km, growth rates of about $6 \times 10^{-3} \text{ s}^{-1}$ can be found, which is in the range of the characteristic time scale, and therefore will not develop into a non-linear stage. If we assume that the ionosphere is unmagnetized, while the induced magnetic

field in the magnetosheath is 30 nT, the maximum growth rate is 0.01 s^{-1} at a wavelength of 100 km. The growth time therefore is 100 s, which is larger than the magnetic barrier formation time.

Global magnetic field measurements of the MGS spacecraft revealed that the strong crustal magnetism is mainly confined to the ancient, heavily cratered highlands in the south (e.g., Connerney et al., 2001). The influence of this local remnant magnetism leads to a strong local curvature of the magnetopause (Ma et al., 2002). If we assume a curvature radius of 400 km, the growth rates at a wavelength of 100 km are about 0.03 s^{-1} . Near the polar terminator, growth rates of 0.015 s^{-1} at 100 km are achieved for an unmagnetized ionosphere and nominal and low solar wind conditions, respectively. If we assume a magnetic curvature radius of $R_m = 400$ km, an induced field of $B_1 = 100$ nT and an ionospheric magnetic field of $B_2 = 30$ nT, the growth rates are about 0.1 s^{-1} for a wavelength of 100 km, corresponding to a growth time of 10 s. At the equatorial flanks, the magnetosheath flow velocities are very high, therefore we consider nominal and low solar wind conditions as in the case for the K–H instability. For a curvature radius of 3750 km, $B_1 = 100$ nT, and $B_2 = 30$ nT, we achieve growth rates of 0.06 and 0.04 s^{-1} for nominal and low solar wind conditions, respectively. For a curvature radius of 400 km, the growth rates at a wavelength of 100 km are found to be 0.15 s^{-1} and 0.1 s^{-1} for nominal and low solar wind velocities, which is much smaller than the characteristic timescale. Additionally, we should keep in mind, that if finite boundary layer effects are considered (Arshukova et al., 2004) the growth rates are likely to become larger. Therefore, it is very likely that the interchange instability appears mainly at the regions with a strongly curved magnetopause due to crustal magnetism, which may trigger an enhanced appearance of plasma clouds in these regions.

7. Discussion and conclusions

In this study we show that the Kelvin–Helmholtz instability has growth rates less than the characteristic frequencies in the terminator region as well as at the equatorial flanks. Therefore, it is very likely that the Kelvin–Helmholtz instability can evolve into a non-linear stage leading to the detachment of plasma clouds in these regions, although the influence of collisions on the evolution of the Kelvin–Helmholtz instability for low solar wind velocities should be considered in future. Additionally, we suppose that in areas where local remnant crustal magnetism leads to a strong curvature of the ionopause, the interchange instability also reaches growth rates less than the characteristic frequencies. This means that in these regions wave-like structures evolve, which can be an additional trigger for the

Kelvin–Helmholtz instability, which may lead to an enhanced appearance of plasma clouds and therefore atmospheric escape associated with regions of strong crustal magnetism. There are indications that on Mars, like on Venus, most of the plasma clouds are found near the terminator, but at the terminator they are already clearly separated from the ionopause, meaning that they may be detached far upstream. An explanation for this observation can be found by including the Hall term in the description of the Kelvin–Helmholtz instability. In this case, the instability arises due to a current related to the sheared cross field ion flow and leads to an instability of the ionopause even in the subsolar region. Penz et al. (2004) showed that detached plasma clouds due to the Kelvin–Helmholtz instability may remove atmospheric particles as efficient as ion pickup and other non-thermal escape processes. But in this work, the interchange instability was not considered. If the interchange instability triggers plasma clouds at regions with crustal magnetism even more particles may be removed from the Martian atmosphere.

Acknowledgements

This work is supported by the Austrian “Fonds zur Förderung der wissenschaftlichen Forschung” under the Project P17099–N08, by the STE Simulation Promotion Program, Nagoya University, by Grant E02–8.0–22 from the Russian Ministry of Higher Education, by Grants 04–05–64088, and 03–05–20014 BNTS a from the Russian Foundation of Basic research, and by Project Nr. I.2/04 from “Österreichischer Austauschdienst”.

References

- Acuña, M.H. et al. Magnetic field and plasma observations at Mars: Initial results of the Mars Global Surveyor mission. *Science* 279, 1676–1680, 1998.
- Arshukova, I.L., Erkaev, N.V., Biernat, H.K., Vogl, D.F. Interchange instability of the Venusian ionopause. *Adv. Space Res.* 33, 182–186, 2004.
- Biernat, H.K., Erkaev, N.V., Farrugia, C.J. MHD effects in the Venus magnetosheath including mass loading. *Adv. Space Res.* 28, 833–839, 2001.
- Brace, L.H., Theis, R.F., Hoegy, W.R. Plasma clouds above the ionopause of Venus and their implications. *Planet. Space Sci.* 30, 29–37, 1982.
- Chandrasekhar, S. *Hydrodynamic and Hydromagnetic Stability*. Oxford Univ. Press, New York, 1961.
- Cloutier, P.A., Tascione, T.F., Daniell Jr., R.E., Taylor, H.A., Wolff, R.S. Physics of the interaction of the solar wind with the ionosphere of Venus: Flow/field models. In: Hunten, D.M., Colin, L., Donahue, T.M., Moroz, V.I. (Eds.), *Venus*. Univ. of Arizona Press, Tucson, pp. 941–979, 1983.
- Connerney, J.E.P. et al. The global magnetic field of Mars and implications for crustal evolution. *Geophys. Res. Lett.* 28, 4015–4018, 2001.
- Elphic, R.C., Ershkovich, A.I. On the stability of the ionopause of Venus. *J. Geophys. Res.* 89, 997–1002, 1984.
- Kliore, A.J. Radio occultation observations of the ionospheres of Mars and Venus. In: Kliore, A.J. (Ed.), *Venus and Mars: Atmospheres, Ionospheres, and Solar Wind Interactions*. American Geophysical Union, Washington, pp. 265–276, 1992.
- Lichtenegger, H.I.M., Lammer, H., Stumptner, W. Energetic neutral atoms at Mars: III. Flux and energy distribution of planetary energetic H atoms. *J. Geophys. Res.* 107 (A10), 1279, 2002.
- Ma, Y., Nagy, A.F., Hansen, K.C., DeZeeuw, D.L., Gombosi, T.I., Powell, K.G. Three-dimensional multispecies MHD studies of the solar wind interaction with Mars in the presence of crustal fields. *J. Geophys. Res.* 107, 1282, 2002.
- Ong, R.S.B., Roderick, N. On the Kelvin Helmholtz instability of the Earth’s magnetopause. *Planet. Space Sci.* 20, 1–10, 1972.
- Penz, T., Erkaev, N.V., Biernat, H.K., Lammer, H., Amerstorfer, U.V., Gunell, H., Kallio, E., Barabash, S., Orsini, S., Milillo, A., Baumjohann, W. Ion loss on Mars caused by the Kelvin–Helmholtz instability. *Planet. Space Sci.* 52, 1157–1167, 2004.
- Rezhnev, B.V., Maltsev, Y.P. Role of interchange instability in flux transfer event origin. *Ann. Geophys.* 12, 183–187, 1994.
- Russell, C.T., Luhmann, J.G., Elphic, R.C., Scarf, F.L., Brace, L.H. Magnetic field and plasma wave observations in a plasma cloud at Venus. *Geophys. Res. Lett.* 9, 45–48, 1982.
- Shinagawa, H., Cravens, T.E. A one-dimensional multispecies magnetohydrodynamic model of the dayside ionosphere of Mars. *J. Geophys. Res.* 94, 6506–6516, 1989.
- Terada, N., Machida, S., Shinagawa, H. Global hybrid simulation of the Kelvin–Helmholtz instability at the Venus ionopause. *J. Geophys. Res.* 107 (A12), 1471–1490, 2002.
- Terada, N., Shinagawa, H., Machida, S. Global hybrid model of the solar wind interaction with the Venus ionopause: ion escape processes. *Adv. Space Res.* 33 (2), 161–166, 2004.
- Thomas, V.A., Winske, D. Kinetic simulation of the Kelvin–Helmholtz instability at the Venus ionopause. *Geophys. Res. Lett.* 18, 1943–1946, 1991.
- Wolff, R.S., Goldstein, B.E., Yeates, C.M. The onset and development of Kelvin–Helmholtz instability at the Venusian ionopause. *J. Geophys. Res.* 85, 7697–7707, 1980.